# The generation of nearly isotropic turbulence downstream of streamwise tube bundles

**P. E. Roach***

Tube bundles were used to generate a field of nearly isotropic turbulence. A wide range of geometric and aerodynamic parameters were systematically studied, with measurements being made of pressure losses, turbulence intensities, spectra, auto-correlations and length scales. Simple analyses were utilized to correlate effectively these results and to aid in their understanding. The results agree well with other (limited) results published in the literature.

**Keywords:** *isotropic turbulence, turbulence generation*

## Introduction

This work originated from a desire to generate moderate levels of turbulence intensity (of order 10%) which might be considered useful in the simulation of turbomachinery turbulence. Moreover, a device was needed which would generate this level of turbulence within a turbine cascade rig operating at geometric, aerodynamic and thermodynamic conditions representative of real gas turbines. Because of these limitations, it was considered that turbulence-generating grids would either not be sufficiently robust or, alternatively, would have to operate at conditions where the flow within the grid is near choking. Also, the rapid decay rate of grid-generated turbulence, especially at turbulence levels of order 10%, was considered too high. Therefore, although a large number of experiments has been reported concerning the turbulence-generating characteristics of grids (see Refs 1 and 2), an alternative device has been examined with which it was hoped the above requirements would be satisfied.

Preliminary measurements made within Rolls-Royce (unpublished) suggested that the use of streamwise, in-line, square-array matrices of tubes (hereafter called tube bundles) might indeed satisfy all the above requirements. For this reason a series of experiments was proposed to describe the aerodynamic characteristics of tube bundles. The aims have been to generate nearly isotropic turbulence of moderate intensity, and to provide sufficient information which would be useful in the design stage of such devices. To this end a wide range of geometric and aerodynamic conditions has been investigated, concentrating on the higher Reynolds number, turbulent flow regime of these devices. Measurements of pressure loss, turbulence intensity, length scales, power spectra and auto-correlations have all been made. The results are analysed by means of simple semi-empirical models where possible.

* Advanced Research Laboratory, Rolls-Royce Ltd, PO Box 31, Derby, DE2 8BJ, UK

Manuscript received 13 June 1985 and accepted for publication on 16 October 1985

Probably the earliest report concerning the use of tube bundles in a wind tunnel was published by Dryden[3]. In this instance the bundles were used to reduce the background turbulence level (of order 1%) and to remove any residual swirl from the wind tunnel inlet. For these reasons, Dryden's results are of limited value to the present work, but nevertheless they are found to be in remarkably good agreement with the turbulence measurements reported in this paper.

Plastic drinking straws have been used by Loehrke and Nagib[4], again to reduce the background turbulence near the inlet of a wind tunnel (of order 6 to 10%). Although a large number of measurements were made downstream of these straw arrays, coupled with some very informative flow visualization, their results are of even less relevance to this work. This is not only because of the very high level of inlet turbulence, but also because their measurements were made at rather low values of Reynolds number, the straws operating within the laminar flow regime.

Krebs *et al*[5] performed an experiment in a water tunnel using a block of material which had a large number of holes drilled along its length. The solidity of their 'jet-block' was 0.325, with a hole length-to-diameter ratio of 17. Reynolds number values were in the turbulent range. Downstream turbulence intensities, micro- and integral length scales and some sample spectra are presented. Their results are discussed further below.

## Experimental equipment

The experimental test rig used in the present work has been carefully designed to present uniform, steady flow to the working section, with a low level of background turbulence intensity. The so-called 'turbulence rig' is shown in Fig 1. The site air supply is fed into the plenum section through a number of flow-manipulating devices to remove oil droplets and other contaminants (about 95% removal of particles larger than 5 $\mu$m), minimize flow inhomogeneity and reduce the velocity fluctuations. A large area contraction ratio between the plenum and

working section (28:1) via a bell-mouth further reduces the background turbulence and provides a suitable means of measuring the upstream flow conditions. The rectangular working section is made of Perspex, and is 50 mm × 76 mm × 610 mm long, with the tube bundle located at the upstream end, as shown in the figure. In the clear duct configuration (ie no tube bundle or other obstruction present), steady mean airflow velocities in the range 10 to 200 m/s are possible (ie Mach numbers from 0.03 to 0.6).

To determine the pressure losses and turbulence properties, a three-dimensional traverse mechanism was located outside the working section, onto which could be mounted either a total pressure probe or a hot-wire probe. By this means, total pressure, mean and fluctuating velocities could all be measured within the Perspex duct anywhere between the duct exit plane and the bundle exit plane. In all the present work the flow was vented to atmosphere at the duct exit plane.

A variety of tube bundles has been used in the present work, covering a wide range of length-to-diameter ratios and porosities. These have been constructed from stainless steel tubes welded together, care being taken to remove excess weld and burrs at both the inlet and exit ends of each tube. Both the inside diameter, $D_i$, and the outside diameter, $D_o$, have been measured accurately by means of a travelling microscope. The surface roughness of the tubes was measured by means of a 'Talysurf' device. The average roughness height (centreline average value) was found to vary between 0.4 and 1.0 $\mu$m, yielding a maximum ratio of roughness height to tube inside diameter of $0.5 \times 10^{-3}$. It has been assumed in all subsequent analysis that the tubes can be considered aerodynamically smooth for the range of flow conditions covered. Table 1 describes the principal bundle dimensions, each bundle having a code number for simplicity.

In this table, $L$ is the tube length, $D_h$ is the hydraulic diameter defined as

$$D_h = \frac{4 \times \text{flow area}}{\text{wetted perimeter}}$$

$$= \frac{4D_o}{\pi}\left\{\frac{1-\frac{\pi}{4}(1-(D_i/D_o)^2)}{1+(D_i/D_o)}\right\}$$

Also, the porosity $\beta$ is defined as

$$\beta = \frac{\text{flow area}}{\text{total duct area}}$$

ie

$$\beta = 1 - \frac{\pi}{4}(1-(D_i/D_o)^2)$$

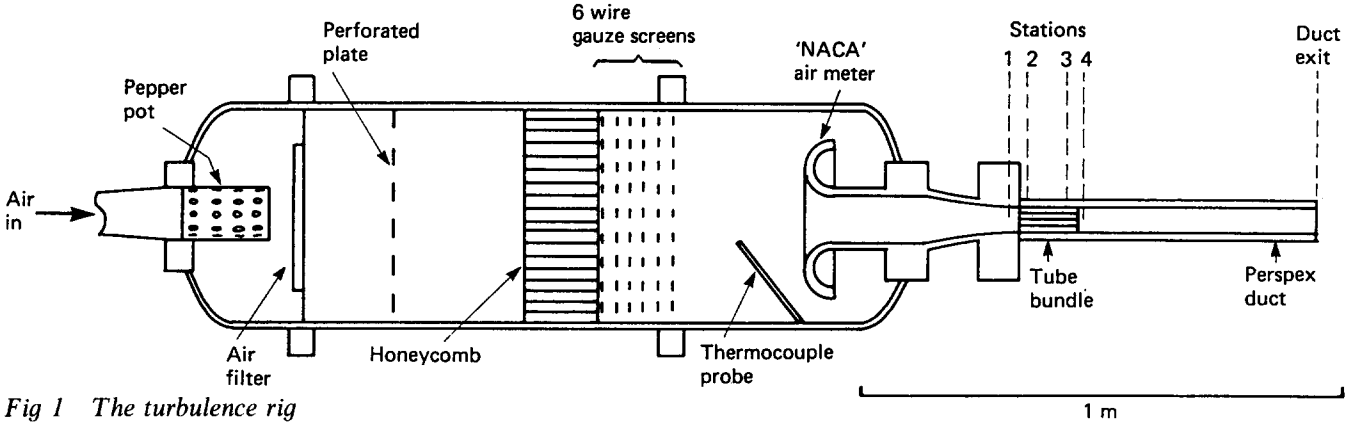


*Fig 1 The turbulence rig*

## Notation

| | |
|---|---|
| $D$ | Diameter |
| $E$ | One-dimensional power spectral density |
| $f$ | Frequency |
| $L$ | Tube length |
| $M$ | Mach number |
| $n$ | Turbulence decay index in Eq (21) |
| $P$ | Total pressure |
| $p$ | Static pressure |
| $q$ | Dynamic pressure |
| $Re$ | Reynolds number |
| $R(T)$ | Auto-correlation coefficient |
| $T$ | Time scale |
| $Tu$ | Streamwise turbulence intensity, $u/U$ |
| $U$ | Streamwise mean velocity |
| $u$ | Streamwise rms fluctuating velocity |
| $\beta$ | Porosity |
| $\Gamma$ | Inlet choking loss factor in Eq (15) |
| $\gamma$ | Ratio of specific heat capacities |
| $\zeta$ | Relaxation factor in Eq (14) |
| $\Lambda$ | Streamwise integral length scale |
| $\lambda$ | Streamwise dissipation length scale |
| $\rho$ | Fluid density |
| $\tau$ | Shear stress |

### Subscripts

| | |
|---|---|
| 1,2,3,4 | Measurement planes in Fig 1 |
| $\infty$ | Value at downstream infinity |
| c | Contraction |
| e | Expansion |
| h | Hydraulic |
| i | Inside |
| min | Value at start of turbulence power law decay |
| o | Outside, or after transition, or virtual origin |
| t | Value at transition |

### Superscripts

| | |
|---|---|
| * | Value at choked condition |
| + | Value beyond choked condition |

**Table 1 Principal bundle dimensions**

| Code | $D_o$ mm | $D_i$ mm | $L$ mm | $L/D_h$ | $\beta$ |
|---|---|---|---|---|---|
| 1/8-6 | 3.13 | 1.86 | 153 | 124 | 0.492 |
| 16-6 | 6.35 | 3.05 | 171 | 79 | 0.396 |
| 16-3 | 6.35 | 3.05 | 76 | 35 | 0.396 |
| 20-6 | 6.38 | 4.34 | 170 | 61 | 0.579 |
| 20-3 | 6.38 | 4.34 | 76 | 27 | 0.579 |
| 1/4-6 | 6.35 | 5.64 | 152 | 42 | 0.834 |
| 1/2-12 | 12.75 | 11.10 | 324 | 46 | 0.810 |
| 1/2-6 | 12.75 | 11.10 | 152 | 22 | 0.810 |

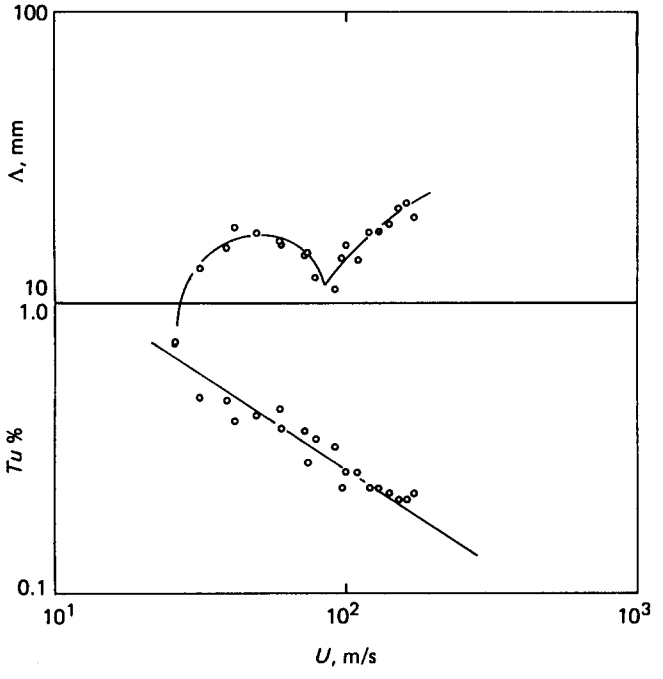


*Fig 2 Background turbulence level in the turbulence rig*

Finally, all the tube bundles have been arranged in a square array matrix.

For all the turbulence measurements, a single hot-wire probe was used (5 $\mu$m diameter, 1.25 mm sensing length) oriented normal to the flow direction. This was coupled to a standard (55D series) DISA constant-temperature anemometry system. Power spectra and auto-correlation measurements were made by means of a Hewlett-Packard HP5420 spectrum analyser, and an FM tape recorder. All the experimental data were recorded on cassette tapes and analysed via a HP9825 desk-top computer.

## Inlet test conditions

The inlet flow conditions were found to be very steady, with an incident boundary layer thickness of order 2 to 3 mm at the start of the Perspex working section. Fig 2 shows the level of the inlet turbulence intensity and integral length scale over a wide range of values of flow velocity. Although the intensity varies from 1% at 20 m/s to 0.16% at 170 m/s, note that the bulk of the turbulence intensity measurements have been made in the velocity range 40 to 100 m/s. This strong Reynolds number dependence is doubtless due to the wire meshes in the plenum of the turbulence rig (see Fig 1).

For each data point shown in Fig 2, one-dimensional power spectra have been measured; a typical spectrum is shown in Fig 3. Assuming the turbulence to be truly homogeneous and isotropic it is possible to fit the spectra with the relationship[6]

$$\frac{4u^2\Lambda}{EU}=1+\left(\frac{2\pi f\Lambda}{U}\right)^2 \tag{1}$$

where $u^2$ is the turbulence energy, $E$ is the power spectral density, $U$ is the mean velocity, $f$ the frequency and $\Lambda$ is the streamwise integral length scale. Eq (1) is known to be inapplicable at high frequencies (typically 20 to 40 kHz) due to assumptions used in its derivation. Numerical results derived from this formula are included in Fig 3 and are seen to fit the experimental data reasonably well, suggesting that the inlet turbulence is nearly isotropic in nature. Now, the integral length scale is derived from the zero-frequency energy level of the measured power spectra; from Eq (1) it can easily be seen that as $f\rightarrow 0$, the length scale is given by

$$\Lambda=\left.\frac{EU}{4u^2}\right|_{f\rightarrow 0} \tag{2}$$

The integral scales so derived (see Fig 2) are found to range between 10 and 20 mm, the only point of interest being the trough found at around 90 m/s. Examination of the spectrum at 91 m/s shows a large tone at 750 Hz, corresponding to a resonance in the pipework upstream of the plenum. This tone is not present at velocities below 80 m/s and above 96 m/s.

For all the recorded spectra the measured and calculated curves were consistently found to diverge at approximately 20–40 kHz. (The bulk of the measurements were limited to frequencies less than 25 kHz, though a small number were made at up to 100 kHz.) From the calibration procedure, the dynamic response of the hot wires used was always better than 10 $\mu$s, which is also within the bandwidth of the linearizer used in the present measurements. It is concluded, therefore, that this deviation is caused by the limitations of Eq (1) already mentioned above.

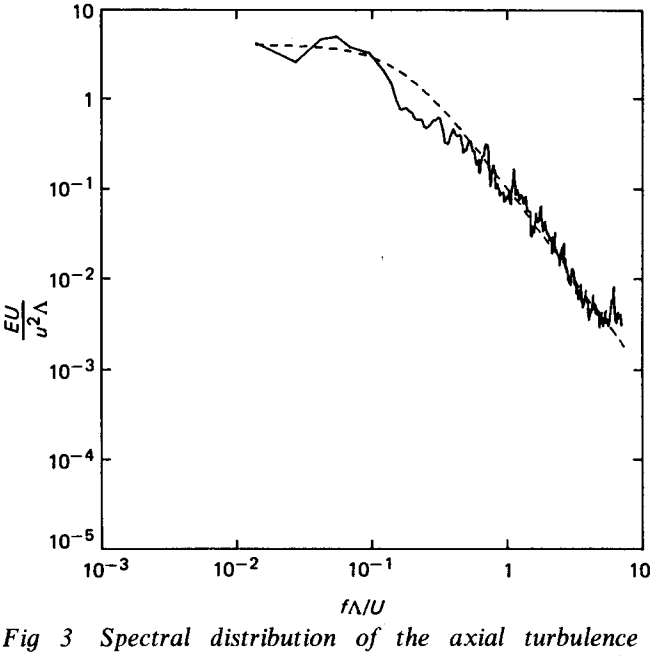


*Fig 3 Spectral distribution of the axial turbulence component (continuous line: clear duct, $U=58.9$ m/s; broken line: analysis, Eq (1))*

## Bundle pressure losses

Figs 4 and 5 present the pressure loss measurements for all the tube bundles tested; the reader should refer to Table 1 for a description of the coding used to define each tube bundle examined. The Reynolds number used here is derived from the inlet velocity (Fig 1, station 1) and the outside diameter of the tubes, the pressure losses being rendered dimensionless by the inlet dynamic pressure. It will be observed that there is a similar trend for each set of data: from the lowest flow rates, the loss rises to a level corresponding to a transition Reynolds number, maintains a plateau level and then rises further under the influence of compressibility.

Although a rigorous mathematical treatment of the flow through a tube bundle is not feasible, it is possible to derive a set of equations with which the pressure losses can be correlated. Referring to Fig 1 it will be seen that three major flow regions can be defined as follows.

(a) The upstream zone between stations 1 and 2: here, it has been assumed that the flow is isentropic, with a pressure loss term added to account for the flow contraction/vena contracta, $\Delta p_c$.

(b) The bundle zone between stations 2 and 3: here, the assumption of isentropic flow has been replaced by one of adiabatic flow in a constant area duct with surface friction, ie Fanno flow.

(c) The downstream zone between stations 3 and 4: the assumption of isentropic flow is reintroduced, again with an additional pressure loss term to account for the flow expansion, $\Delta p_e$.

Assuming the flow is steady, one-dimensional and has uniform flow conditions at both stations 1 and 4, and applying the conservation of momentum, mass and energy, the following equation is derived for the pressure loss coefficient:

$$\frac{\Delta p}{q}=\lambda\frac{Lq_2}{D_h q_1}+\frac{\Delta p_c}{q_1}+\frac{\Delta p_e}{q_1}$$
$$+2\left\{\frac{1-\beta}{1+\beta}\right\}\left\{\frac{q_3}{q_2}-1\right\}\frac{q_2}{q_1}+\frac{4\zeta}{(1+\beta)}\left\{\frac{q_4}{q_1}-1\right\} \quad (3)$$

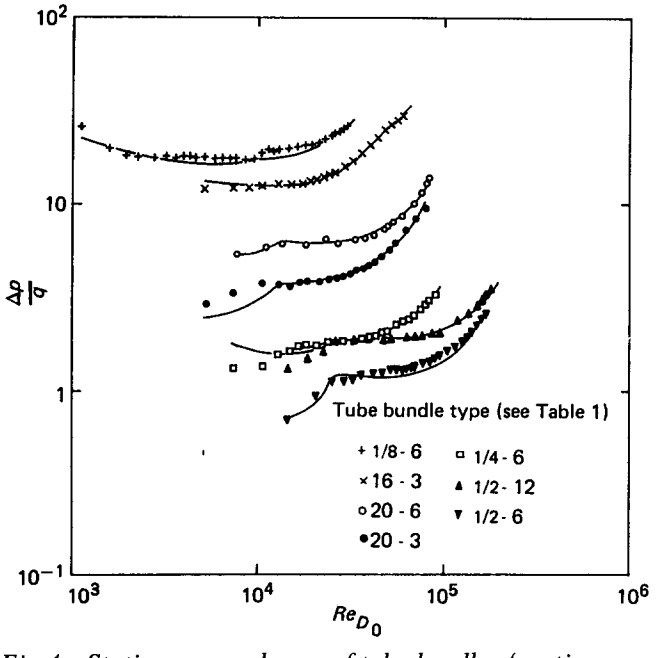


*Fig 4 Static pressure losses of tube bundles (continuous lines: analysis)*

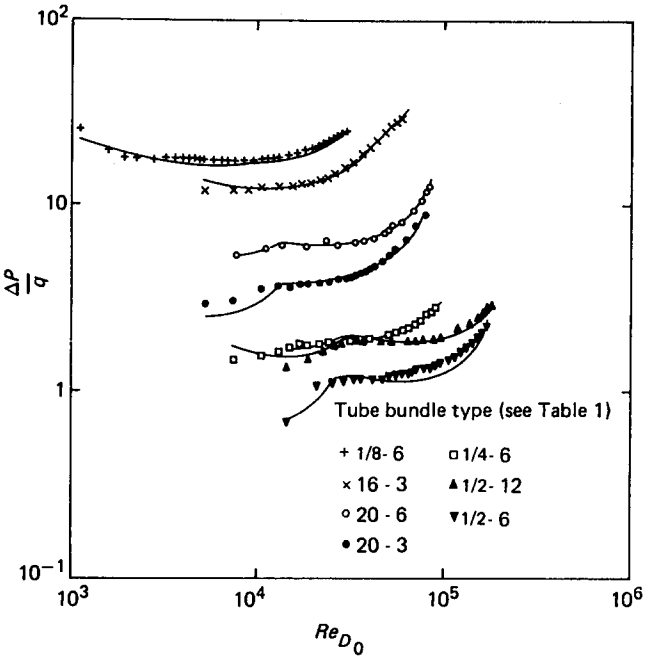


*Fig 5 Total pressure losses of tube bundles (continuous lines: analysis)*

In this equation, $\Delta p/q \equiv (p_1 - p_4)/q_1$, $p$ is the static pressure, $q$ the dynamic pressure $(1/2\rho U^2)$, $\beta$ is the bundle porosity, $L$ its length and $D_h$ its hydraulic diameter, $\lambda$ is the friction factor and the subscripts denote the planes indicated in Fig 1. The remaining term $\zeta$ has been added because the above analysis assumes that the velocity at the bundle exit plane is uniform, ie there has been no boundary layer growth within the individual tubes. In reality this is obviously not the case, and hence an additional factor is necessary to account for the relaxation of the profiles to a uniform velocity by station 4. The friction factor $\lambda$ is defined by

$$\lambda = 4\tau/q_2$$

where $\tau$ is the mean shear stress within the tubes.

It is seen that there are seven unknown in Eq (3) which need to be determined: $q_2$, $q_3$, $q_4$, $\lambda$, $\Delta p_c$, $\Delta p_e$ and $\zeta$. Assuming isentropic flow and that the total pressures $P_1$ and $P_2$ are equal, the following pair of equations is obtained:

$$\frac{M_2}{M_1}=\frac{1}{\beta}\left\{\frac{1+\left(\frac{\gamma-1}{2}\right)M_2^2}{1+\left(\frac{\gamma-1}{2}\right)M_1^2}\right\}^{(\gamma+1)/2(\gamma-1)} \quad (4)$$

$$\frac{q_2}{q_1}=\frac{1}{\beta^2}\left\{\frac{1+\left(\frac{\gamma-1}{2}\right)M_2^2}{1+\left(\frac{\gamma-1}{2}\right)M_1^2}\right\}^{1/(\gamma-1)} \quad (5)$$

where $\gamma$ is the ratio of specific heat capacities, taken to be 1.40 here. So, Eq (4) may be solved iteratively to find $M_2$, knowing $M_1$, then $q_2$ can be determined from Eq (5).

Assuming Fanno flow between stations 2 and 3 it is possible to estimate $q_3$. First, the bundle exit plane Mach

number $M_3$ is derived from

$$\frac{1}{M_3^2}=\frac{1}{M_2^2}+\left(\frac{\gamma+1}{2}\right)\ln\left\{\left(\frac{M_2}{M_3}\right)^2\left(\frac{1+\left(\frac{\gamma-1}{2}\right)M_3^2}{1+\left(\frac{\gamma-1}{2}\right)M_2^2}\right)\right\}$$

$$-\gamma\left\{\lambda\frac{L}{D_h}+\Gamma\right\} \tag{6}$$

Note that the final term in Eq (6) is made up of the frictional pressure loss and a further pressure loss $\Gamma$ which is associated with the developing boundary layers near the inlets of the tubes. This loss needs to be determined empirically, thus adding a further unknown (see below for further comment).

Having determined $M_3$ from Eq (6), $q_3$ is given by

$$\frac{q_3}{q_2}=\left(\frac{M_3}{M_2}\right)^{1/2}\left\{\frac{1+\left(\frac{\gamma-1}{2}\right)M_2^2}{1+\left(\frac{\gamma-1}{2}\right)M_3^2}\right\}^{1/2} \tag{7}$$

The final dynamic pressure, $q_4$, can be determined by assuming sudden expansion flow. After much manipulation, it can be shown that

$$\frac{q_4}{q_1}=\frac{\gamma}{(\gamma+1)}\frac{q_3}{q_1}Q\left\{1-\left[1-\frac{(\gamma^2-1)\beta^2}{\gamma^2 Q}\left(\frac{1}{(\gamma-1)M_3^2}+1\right)\right]^{1/2}\right\} \tag{8}$$

where

$$Q=\frac{\Delta p_e}{2q_3}+\frac{1}{\gamma M_3^2}+\beta \tag{9}$$

The inlet and exit pressure losses have already been determined both analytically and experimentally by Kays[7]. Considering only the incompressible turbulent flow regime, his experimental findings show:

$$\frac{\Delta p_c}{q_2}=\frac{1}{2}(1-\beta) \tag{10}$$

and

$$\frac{\Delta p_e}{q_3}=(1-\beta)^2 \tag{11}$$

Note that these relationships are found to agree well with Kays's data for all the tube shapes used in his experiments; square, circular and triangular 'tubes' were examined.

The friction factor $\lambda$ has been assumed to obey the relationship,

$$\lambda=aRe_{D_h}^{-\frac{1}{4}} \tag{12}$$

where $Re_{D_h}=U_2D_h/\nu$, and the 'constant', $a$, must be determined empirically. The present results suggest

$$a=0.47(1-\beta)^{-0.17}\left(\frac{L}{D_h}\right)^{-\frac{1}{5}} \tag{13}$$

Note that because the tube bundles used here are rather short, there is a strong influence of the inlet flow included in the 'constant' $a$.

The wake relaxation factor $\zeta$, determined empirically, is given by,

$$\zeta=1+\frac{1}{30}\left\{\frac{1}{\beta^2}+1\right\}^2 \tag{14}$$

The loss parameter $\Gamma$ is purely an empirical addition that has been generated to give choked flow at the bundle exit plane to within $\pm 1\%$ of the measured upstream choking Mach number, $M_1^*$. The results suggest

$$\Gamma=2.65\left(\frac{L}{D_h}\right)^{-\frac{1}{2}} \tag{15}$$

Beyond choking, the mass flow rate reaches a maximum and the nature of the loss-generating mechanisms alters completely. Then a further assumption is necessary: the one made here is that on increasing the upstream pressure beyond the level at choking, a significant proportion of this pressure increase is lost, independent of bundle geometry. A suitable empirical factor for this proportion is 50%. Therefore, beyond choking,

$$\frac{\Delta p}{q}=\frac{\Delta p^*}{q}+\frac{1}{2}\frac{\Delta p^+}{q} \tag{16}$$

where $\Delta p^*$ is the pressure loss at the choked condition, $\Delta p^+=p_1-p_1^*$, and $p_1^*$ is the inlet pressure at the choked condition.

When the Reynolds number drops below a critical value a different flow regime comes into being, composed of transitional flow within the tubes and/or at the inlet/exit of the tubes. The present results show the critical Reynolds number $(U_2D_h/\nu)$ to be around $10^4$, much higher than might be expected for transition in fully developed pipe flow. It has therefore been assumed here that it is only the inlet (vena contracta) flow region that is transitional, at least above Reynolds numbers of order $10^3$. This upper transition Reynolds number is well described by

$$Re_{D_t}\equiv\left.\frac{U_1D_o}{\nu}\right|_t=4\times10^4\beta^2 \tag{17}$$

where subscript t denotes transition. The fact that the transition Reynolds number appears to be independent of the tube length:diameter ratio also confirms that this is an inlet flow effect. Below this Reynolds number the inlet loss has been fitted empirically and is reduced according to

$$\frac{\Delta p_c}{q}=\frac{\Delta p_\infty}{q}\left\{g\log_{10}^{-1}\left(\frac{Re_D}{Re_{D_t}}\right)-10g+1\right\} \tag{18}$$

where

$$g=1-1.4(1-\beta) \tag{19}$$

and the zero subscript denotes the pressure loss beyond transition (Eq 10).

Not only is the loss in static pressure of interest; a knowledge of the loss in total pressure also provides useful information. At low Mach numbers (strictly, zero Mach number) these two quantities are equal, but at higher Mach numbers the total pressure loss is less than the static pressure loss. This difference can be accounted for in the following manner. With

$$\frac{P_1}{p_1}=\left(1+\left(\frac{\gamma-1}{2}\right)M_1^2\right)^{\gamma/(\gamma-1)}$$

and

$$\frac{P_4}{p_4}=\left(1+\left(\frac{\gamma-1}{2}\right)M_4^2\right)^{\gamma/(\gamma-1)}$$

then rearranging and expanding the terms in brackets (ignoring higher order terms),

$$P_1 - P_4 \approx p_1 - p_4 + \frac{\gamma}{2}(p_1 M_1^2 - p_4 M_4^2)$$

that is,

$$\frac{\Delta P}{q} \equiv \frac{P_1 - P_4}{q_1} \approx \frac{\Delta p}{q} + \left(1 - \frac{q_4}{q_1}\right) \tag{20}$$

This appears to agree reasonably well with the present findings.

Eqs 3 to 20 constitute a closed set of relationships, the results of which are included in Figs 4 and 5 for comparison with the experimental results, the bulk of the data being within $\pm 10\%$ of the calculations. Since such a large range of both geometric and aerodynamic conditions have been examined, and such simple assumptions have been used in the model, this agreement is quite satisfactory.

## Downstream turbulence characteristics

### Turbulence intensities

From dimensional arguments it may be expected that the turbulence intensity $Tu$ downstream of a tube bundle will be a function of the distance downstream, $x$, the geometry of the bundle, the flow Reynolds number and, possibly, Mach number. Now, Naudascher and Farell[1] (hereafter denoted by N&F) suggest that by considering homogeneous, near-isotropic turbulence it is possible to write,

$$Tu Re_D = C\left\{\frac{x - x_0}{D Re_D}\right\}^{-n} \tag{21}$$

where $Tu$ is the ratio of the rms fluctuating velocity ($u$) to the time-mean velocity ($U$), $x_0$ is the location of the virtual origin of the beginning of the power law decay region, $n$ is the power law index, $C$ is an empirical constant, $D$ is some dimension of the turbulence generator in use, and $Re_D$ is a Reynolds number. Note that N&F assumed self-preservation of the turbulence field, making $n = 0.5$. Numerous experiments involving grids and other turbulence generators have shown, however, that truly self-preserving turbulence is seldom realized; therefore, $n$ will be left as an unknown for the present. Note that at a fixed distance downstream, Eq (21) shows that

$$Tu \propto Re_D^{(n-1)} \tag{22}$$

Examination of a selection of the present data confirms this trend. Fig 6 shows that, for a fixed downstream location, with $Re_{D_0}$ greater than $10^4$, the value of $(n-1)$ is $-0.25$, that is $n = 0.75$.

Returning to Eq (21), the remaining constant of proportionality, $C$, must be determined, together with the location of the virtual origin, $x_0$. All the present measurements (for turbulent Reynolds number flows only) are shown in Fig 7. The results are seen to collapse very well onto a single curve, shown in the figure, which is well fitted by the relationship

$$Tu Re_{D_0} = 3.5\left\{\frac{x}{D_0 Re_{D_0}} - 7.5 \times 10^{-5}\right\}^{-\frac{3}{4}} \tag{23}$$

Note that the dimension-eliminating length scale used is the outside diameter of the tubes, and the Reynolds number is that employed elsewhere in this paper, $U_1 D_0/\nu$. The location of the virtual origin is seen to be a function of Reynolds number, in accordance with N&F.

Also note that the data deviate from Eq (23) below some minimum value of $x/D_0 Re_{D_0}$. This minimum is adequately described by

$$\frac{x_{min}}{D_0 Re_{D_0}} \approx 2 \times 10^{-4}$$

or

$$\frac{x_{min}}{x_0} \approx 2.7 \tag{24}$$

A few measurements have been made upstream of this minimum distance (not presented here) which show the

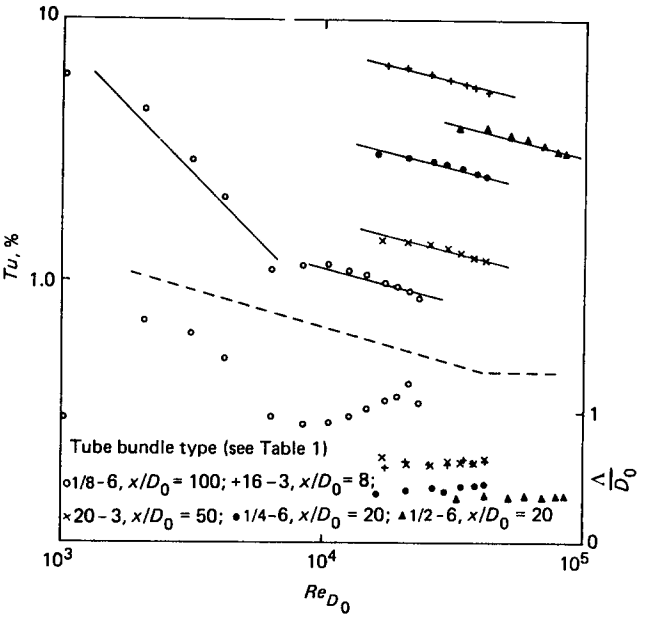


*Fig 6 Reynolds number dependence of the generated turbulence*

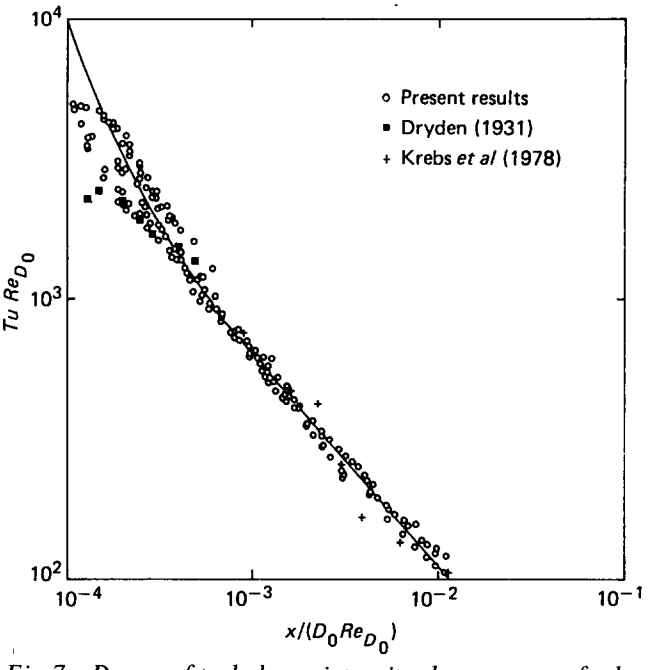


*Fig 7 Decay of turbulence intensity downstream of tube bundles*

expected nonhomogeneous nature of the flow due to the tube boundary layers and wakes.

Finally, the results of Dryden[3] and Krebs *et al*[5] are included in Fig 7, the agreement with the present results being remarkably good. Note that the data of Dryden have been obtained by measuring the turbulence properties of the flow downstream of one tube bundle and two honeycombs, all of which had a length-to-diameter ratio of order 4 to 5. Also, to allow the results of Krebs *et al* to be included, the hole diameter of their 'jet-block' has been used in place of $D_o$.

## Auto-spectra and auto-correlations

A typical one-dimensional power spectrum downstream of a tube bundle is shown in Fig 8, with an auto-correlation shown in Fig 9. In these figures, $f$ is the frequency and $E$ is the power spectral density, rendered dimensionless by the mean velocity $U$, the streamwise turbulence energy, $u^2$, and the integral length scale $\Lambda$. $T$ is the time delay, and the auto-correlation coefficient $R(T)$ is defined as

$$R(T)=\frac{\overline{u(t)u(t-T)}}{u^2} \tag{25}$$

The 'calculated' curves are derived from formulations suggested in Hinze[6], using the measured integral scale (see below). The realtionship for the power spectrum has already been given in Eq (1). For the auto-correlation, the relationship used is

$$R(T)=\exp(-UT/\Lambda) \tag{26}$$

It must be noted that these formulae only apply to strictly homogeneous, isotropic turbulence in a uniform velocity flow field, and even then they do not apply for very high frequencies or very small time delays. Nevertheless, they are seen to agree remarkably well with the present results, suggesting that the generated turbulence is indeed nearly isotropic.

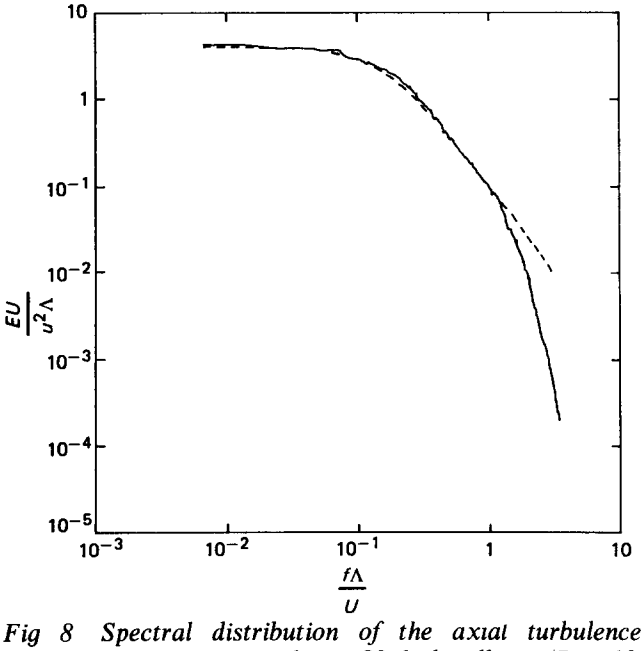


*Fig 8 Spectral distribution of the axial turbulence component (continuous line: 20-6 bundle, $x/D_o=12$, $U=87.5$ m/s; broken line: analysis, Eq (1))*

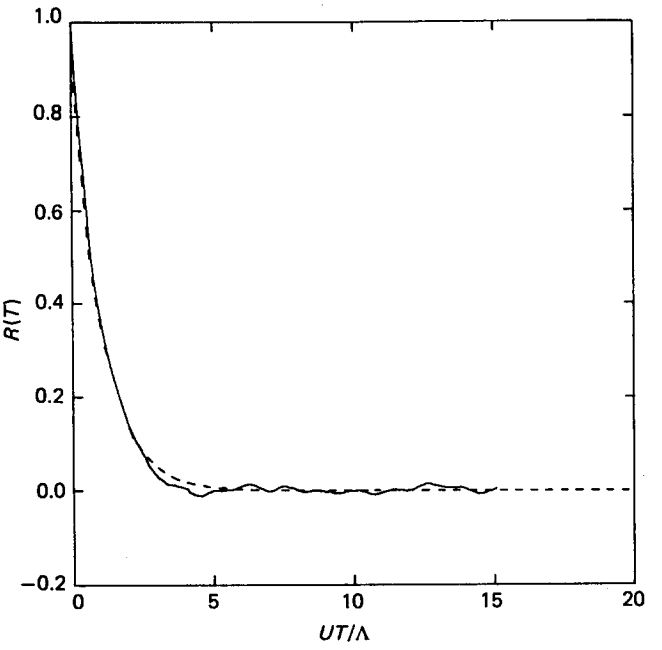


*Fig 9 Auto-correlation of the axial turbulence component (continuous line: $\frac{1}{4}$-6 bundle, $x/D_o=35$, $U=86.0$ m/s; broken line: analysis, Eq (26))*

## Turbulence length scales

Turbulence length scales can be determined, which provide further information regarding the properties of a turbulent fluid flow. Two of the more commonly quoted length scales are discussed here; other scales are described fully by Hinze[6].

The integral or macro-length scale $\Lambda$ may be considered a measure of the largest eddy size in a turbulent fluid. There are a number of methods of measuring this length scale; since only a single hot-wire was used in the present work, the streamwise component of the integral scale, $\Lambda$, may be determined from the auto-correlation function, $R(T)$, given in Eq (25) above. Thus, by definition,

$$\Lambda=U\int_0^\infty R(T)\,dT \tag{27}$$

Assuming the turbulence field can be considered truly homogeneous and isotropic it is also possible to determine this integral scale from the power spectrum, by means of Eq (2). Initial comparisons of a large number of auto-correlation-derived and spectrum-derived length scales showed that there was no systematic difference between the two methods. This adds further proof that the turbulence field downstream of the tube bundles is indeed reasonably homogeneous and isotropic. Therefore the spectrum derivation was used for the majority of the measurements, though it is possible that the error in estimating the integral scale by this means is as large as $\pm 10\%$, owing to some arbitrariness in its determination (extrapolation to $f=0$ Hz).

To correlate the present results, the analysis of N&F has been found to be most suitable. They show

$$\frac{d\Lambda}{dx}=CTu$$

where $C$ is a function of Reynolds number. After integration and rearrangement using Eq (23) we get

$$\frac{\Lambda}{D_o}=\frac{\Lambda_o}{D_o}+D\left\{\frac{x}{D_oRe_{D_o}}-\frac{x_o}{D_oRe_{D_o}}\right\}^{\frac{1}{4}} \tag{28}$$

where $\Lambda_o$ is an initial integral scale (itself a function of Reynolds number) and $x_o$ is the same as that given by Eq (23). The present results suggest the following relationship:

$$\frac{\Lambda}{D_o}=0.85\log_{10}\{Re_{D_o}-6.8\times10^3\}-3.9$$
$$+\left\{\frac{x}{D_oRe_{D_o}}-7.5\times10^{-5}\right\}^{\frac{1}{4}}\{27.3-5.24\log_{10}Re_{D_o}\}$$
$$=F \text{ in Fig 10} \tag{29}$$

The results are shown in Figs 6 and 10, and it is seen that the bulk of the data lie within $\pm20\%$ of Eq (29). This degree of scatter is thought to be quite acceptable, especially since the estimated error in the derivation of $\Lambda$ is itself possibly as large as 10%.

Also included in Fig 10 are the results of Krebs *et al*[5]. Their measurements are seen to be in fairly good agreement with the present results.

The dissipation- or micro-scale $\lambda$ may be considered a measure of the average dimensions of the eddies which are mainly responsible for the dissipation of turbulence energy. As with the integral scale there are a number of methods of determining this dissipation length scale. By definition, the streamwise micro-scale $\lambda$ is given by

$$\frac{1}{\lambda^2}=-\frac{1}{2U^2}\left\{\frac{\partial^2R(T)}{\partial T^2}\right\}_{T=0} \tag{30}$$

Alternatively, if the turbulence field is considered truly homogeneous and isotropic it is possible to determine this micro-scale from the power spectrum. Thus,

$$\frac{1}{\lambda^2}=\frac{2\pi^2}{U^2u^2}\int_0^\infty f^2E\,df \tag{31}$$

As with the integral scale, initial comparisons of the auto-correlation-derived and spectrum-derived microscales showed no systematic difference between the two methods. However, as can be seen from Eq (31), the micro-scale is heavily weighted towards the higher frequencies in the power spectrum. Clearly, therefore, it is possible to determine this length scale incorrectly by measuring the power spectrum at insufficiently high frequencies (or by measuring the auto-correlation function at insufficiently small time delays). A typical power spectrum was examined in order to determine the minimum frequency range necessary to define the micro-scale accurately. Eq (31) was used to compute the micro-scale, the upper frequency limit being reduced from 102.4 kHz (the maximum used in this study), to 20 kHz. Relative to the 102.4 kHz level, the indicated micro-scale obtained over 80 kHz was 1.3% too large, 6.4% over 60 kHz, 20% over 40 kHz, and 71% over 20 kHz! Thus, it is seen that to obtain sensible estimates of the micro-scale it is necessary to determine the power spectrum over at least 80 kHz, preferably over an even larger range of frequencies.

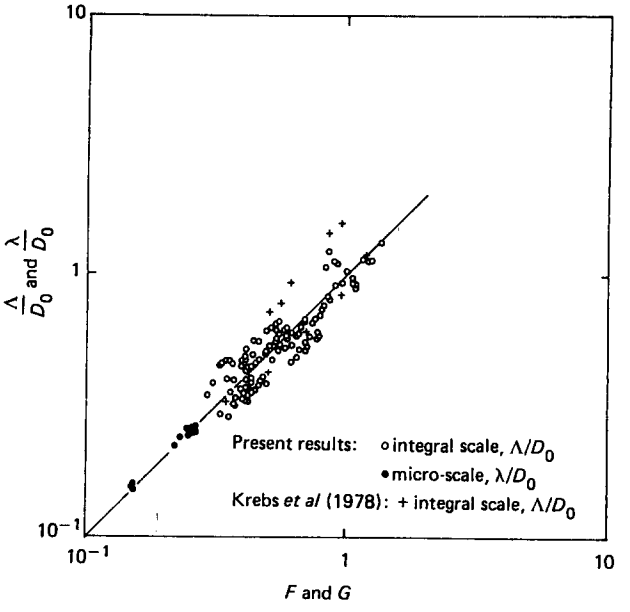


*Fig 10 Integral and micro-length scales downstream of tube bundles*

Again, correlation of the present results has been achieved by means of the analysis of N&F. By assuming that the micro-scales approach a final value, $\lambda_\infty$, as $x\to\infty$, then the following equation is derived:

$$\frac{\lambda}{D_o}=\frac{\lambda_\infty}{D_o}-\frac{K}{Re_{D_o}^{3/2}}\left\{\frac{x}{D_oRe_{D_o}}-\frac{x_o}{D_oRe_{D_o}}\right\}^{-\frac{3}{4}} \tag{32}$$

where $K$ is a constant. The present results suggest the following relationship:

$$\frac{\lambda}{D_o}=\frac{705}{Re_{D_o}^{3/4}}-\frac{150}{Re_{D_o}^{3/2}}\left\{\frac{x}{D_oRe_{D_o}}-7.5\times10^{-5}\right\}^{-\frac{3}{4}}$$
$$\equiv G \text{ in Fig 10} \tag{33}$$

These results are shown in Fig10, and it is seen that the data lie within $\pm5\%$ of Eq 33. Note that only a limited number of measurements were made over the 102.4 kHz frequency range, and it is for this reason that so few data are shown in the figure (the bulk of the measurements have been made over a 25 kHz frequency range).

The micro-scales measured by Krebs *et al*[5] are not included in Fig 10 since their results are considerably larger than the present data (roughly a factor of 2 on $\lambda$). At first sight this would seem to be very surprising since the scale of their experimental arrangement and the Reynolds numbers they used are much the same as in the present arrangement, and their measured turbulence intensities and integral scales are in very good agreement with the present data. The reason for this discrepancy, however, has already been hinted at above, where it was shown that a sufficiently large frequency range is necessary to determine accurately the micro-scale. Krebs *et al* appear to have limited their power spectrum measurements to frequencies below 10 kHz.

## Conclusions

A parametric study of the aerodynamic characteristics of streamwise tube bundles has been completed. For a wide range of values of tube bundle length-to-diameter ratio and porosity, flow Reynolds and Mach numbers, pressure

losses and turbulence characteristics have been determined and simple design rules formulated.

Although turbulence intensity levels of order 10% have been generated, the decay rate was found to be higher than that associated with grid-generated turbulence: $Tu \propto x^{-\frac{1}{2}}$ compared with a grid decay rate, $Tu \propto x^{-\frac{5}{6}}$.

The present results have been compared with other limited measurements in the literature, and found to be in good agreement.

## Acknowledgements

The author would like to thank Rolls-Royce Limited for permission to publish this paper, and his colleagues at the Advanced Research Laboratory for their contributions. This work was financially supported by the Ministry of Defence.

## References

1. **Naudascher E. and Farell C.** Unified analysis of grid turbulence. *Proc. ASCE, 1970, J. Eng. Mech. Div. EM2, 121–141*
2. **Laws E. M. and Livesey J. L.** Flow through screens. *Ann. Rev. Fluid Mech., 1978,* **10**, *247–266*
3. **Dryden H. L.** Reduction of Turbulence in Wind Tunnels. *NACA Report 392, 1931*
4. **Loehrke R. I. and Nagib H. M.** Experiments on Management of Free-Stream Turbulence. *AGARD-R-598, 1972*
5. **Krebs L. Bremhorst K. and Müller U.** Measurements of thermal diffusion downstream of a multi-bore jet block. *Lecture Notes in Physics, 1978,* **76**(*II*), *101–112*
6. **Hinze J. O.** *Turbulence—Introduction to its Mechanism and Theory. McGraw-Hill, 1959*
7. **Kays W. M.** Loss coefficients for abrupt changes in flow cross-section with low Reynolds number flow in single and multiple tube systems. *Trans. ASME, Nov 1950, 1067–1074*



# BOOK REVIEW

## Numerical Methods in Heat Transfer Vol III

Eds R. W. Lewis and K. Morgan

The 13 chapters in this book consist of invited contributions arising from papers presented at the Third International Conference on Numerical Methods in Thermal Problems, held at Seattle in 1983. The book contains a useful blend of new computational modelling techniques and standard methods. In almost all cases, numerical results are presented of flows and heat transfer in real engineering situations.

All but one of the chapters employ either finite element (FE) or finite difference (FD) methods. Two chapters deal with welding problems using FE methods. Of these, one uses an implicit integration scheme for the calculation of transient thermal stresses caused by the highly localized heating and cooling of arc-welding. The other is concerned with automatic butt-welding and identifies the importance of the gap between the tack-welded plates in front of the arc. In another contribution, FE 'engineering elements' are presented which can be used for the analysis of the three modes of heat transfer in problems involving complex geometries; examples are given of flows inside a conducting pipe and between two surfaces of 'inverted cup' shape.

Problems which arise in reservoir engineering of mass and heat transfer in porous media is the subject of one chapter. Particular emphasis is given to minimizing numerical diffusion effects. Another chapter uses FE methods in dealing with the important problem of the non-isothermal extrudate swell of elastic liquids which occurs in polymer processing. Earlier work is extended to cover liquids with significant elasticity, with the 'melt-spinning' of nylon-6 chosen as the numerical example.

Seven of the chapters use various finite difference methods. In the first, an inverse formulation is presented to solve the problem of a moving boundary in phase change calculations. A novel approach is used which allows convergence to be obtained about the singular point where the solidification front meets a boundary. Transient heat transfer in typical structural elements found in (aero)space constructions is analysed in another paper by coupling finite difference solutions in the 'skin' of the elements with exact Laplace transform solutions in the 'web' of the elements.

Calculations are made of natural convection flows in enclosures in two chapters. In the first, block ADI methods are extended and applied to the classical unitary square cavity. The vorticity and stream function are solved both together with and separately from the temperature equation. A useful computer listing of a general block-tridiagonal solution routine is provided. The second paper studies natural convection in tilted enclosures, such as those found in solar collectors, both with and without radiation effects. Such effects are found to be significant.

There are two chapters which use FD methods to calculate combustion phenomena in or near porous material. One addresses the problem of ignition in unmixed gases in the stagnation region of a bluff body by a hot surface when fuel is injected through a porous